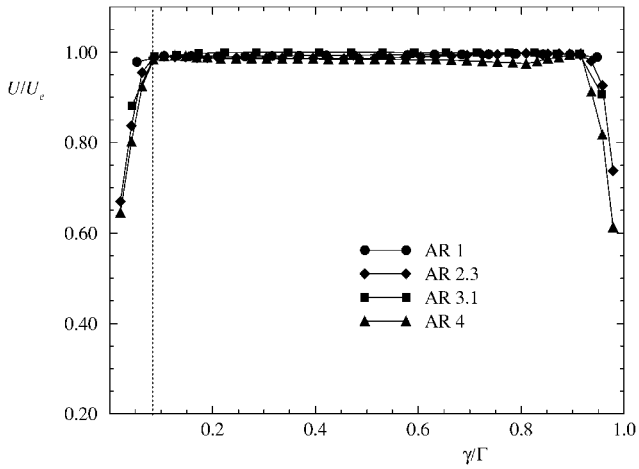

Fig. 4 Diagonal mean velocity profiles.

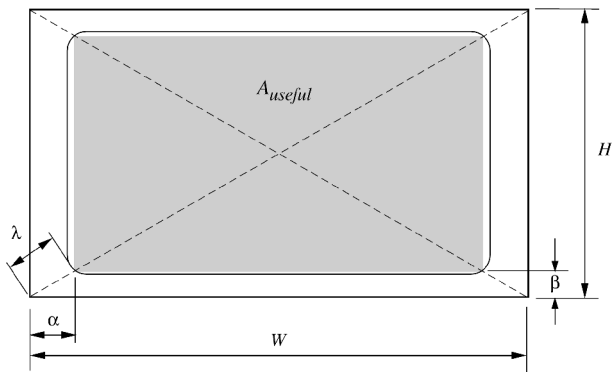

Fig. 5 Useful area of exit plane.

where λ, α, and β are shown in Fig. 5. The total cross-sectional area is $A = WH$, whereas the useful area is defined as $A_{\text{useful}} = (W - 2\alpha)(H - 2\beta)$. When Eq. (4) is used, the useful area becomes

$$A_{\text{useful}} = A(1 - 2C)^2 \approx 0.69A \tag{5}$$

Therefore, the estimated useful cross-sectional working area is a fixed proportion of the total cross-sectional area and has no dependence on AR. Likewise, conservative estimates for useful width and height are also independent of AR: $W_{\text{useful}}/W = H_{\text{useful}}/H \approx 0.83$.

IV. Conclusions

An experimental and computational analysis of the effect of changing the aspect ratio through a three-dimensional wind-tunnel contraction has been performed. Exit flow boundary layers were measured for four contractions ranging from AR 1 to 4, all with equivalent lengths and contraction ratios. Their development was related to the pressure history on the walls, as well as to the related effect of streamline convergence. Comparisons between contractions with different AR show that streamline convergence effects as well as pressure histories need to be considered when performing comparisons of boundary-layer thicknesses on the same wall of the contraction. For a given AR, the side wall boundary layer was found to be thicker than the floor boundary layer for AR > 1. The 45-deg corner boundary-layer thicknesses were found to decrease with increasing AR, consistent with the corner pressure distribution induced by the streamline convergence effects.

An examination of the mean velocity profile along the diagonal of the exit plane reveals a collapse of data. From this, an approximate design rule for the estimation of useful area in the working section has been proposed. For the contraction parameters considered in this study, the useful area is found to be $0.69A$, and this result is independent of AR.

Acknowledgments

The authors were supported by the National Science Foundation through Grants CTS-9983933 and ACI-9982274, and this is gratefully acknowledged.

References

[1]Morel, T., "Comprehensive Design of Axisymmetric Wind Tunnel Contractions," *Journal of Fluids Engineering*, Vol. 97, No. 1, 1975, pp. 225–233.

[2]Su, Y., "Flow Analysis and Design of Three-Dimensional Wind Tunnel Contractions," *AIAA Journal*, Vol. 29, No. 11, 1991, pp. 1912–1920.

[3]Mikhail, M. N., "Optimum Design of Wind-Tunnel Contractions," *AIAA Journal*, Vol. 17, No. 5, 1979, pp. 471–477.

[4]Fang, F. M., "Design Method for Contractions with Square End Sections," *Journal of Fluids Engineering*, Vol. 119, No. 2, 1997, pp. 454–458.

[5]Tulapurkara, E. G., and Bhalla, V. V. K., "Experimental Investigation of Morel's Method for Wind Tunnel Contractions," *Journal of Fluids Engineering*, Vol. 110, No. 1, 1988, pp. 45–47.

[6]Callan, J., "The Effect of a Changing Aspect Ratio Through a Wind Tunnel Contraction," M.S. Thesis, Aerospace Engineering, Univ. of Minnesota, Minneapolis, MN, 2000.

[7]Zamir, M., and Young, A. D., "Experimental Investigation of the Boundary Layer in a Streamwise Corner," *Aeronautical Quarterly*, Vol. 21, Nov. 1970, pp. 313–339.

[8]Bradshaw, P., "Effects of Streamline Curvature on Turbulent Flow," AG-169, AGARD, 1973.

[9]Saddoughi, S. G., and Joubert, P. N., "Lateral Straining of Turbulent Boundary Layers. Part 1. Streamline Divergence," *Journal of Fluid Mechanics*, Vol. 229, 1991, pp. 173–204.

[10]Nakamura, I., Miyata, M., Kushida, T., and Kagiya, Y., "An Experimental Study of the Intermittant Region of a Corner Turbulent Boundary Layer," *Japan Society of Mechanical Engineers International Journal*, Vol. 30, No. 259, 1987, pp. 72–79.

A. Plotkin
Associate Editor

New ν_t–k Model for Calculation of Wall-Bounded Turbulent Flows

Seong Hoon Kim* and Myung Kyoon Chung†
Korea Advanced Institute of Science and Technology, Taejon 305-701, Republic of Korea

Introduction

HISTORICALLY, the Boussinesq eddy viscosity that is assumed for Reynolds shear stress has been indirectly assessed by estimating the velocity scale and length scale of turbulent energetic eddies. Physical models to find these scales were the mixing length model,[1] the one-equation model employing the k equation of Bradshaw et al.,[2] and the two-equation model using the k–ε equations of Jones and Launder[3] or the k–ω equations of Wilcox.[4] More recently, the one-equation model has reemerged by Baldwin and Barth[5] and Spalart and Allmaras.[6] Instead of the k equation, however, they proposed to solve the ν_t equation to assess directly the eddy viscosity. Subsequently, Durbin et al.[7] and Menter[8] formulated other forms of ν_t equations.

To avoid the problem in the one-equation model that the length scale needs to be provided externally, these one-equation models use the von Kármán length scale, $L_{vK} \equiv |S/\nabla S|$, where S is the mean rate of strain, or a composite length scale,[7] ($|\nabla \nu_t/S|$). Because of the advantages of directness of eddy viscosity assessment, simplicity in numerical computation, and use of natural boundary condition for the ν_t equation, the one-equation model has often been a preferred choice in aerodynamic calculations. However, such one-equation models have the following three serious problems. One is that the length scale defined in any of the two methods mentioned earlier varies physically unrealistically in both the near-wall layer and the core region. The second problem is that predicted ν_t varies as y^4 as $y \to 0$ (Fig. 1). The third problem is that when the one-equation

Received 28 November 2000; revision received 23 April 2001; accepted for publication 14 May 2001.

*Graduate Student, Department of Mechanical Engineering, 373-1, Kusong-dong, Yusong-gu.

†Professor, Department of Mechanical Engineering, 373-1, Kusong-dong, Yusong-gu.

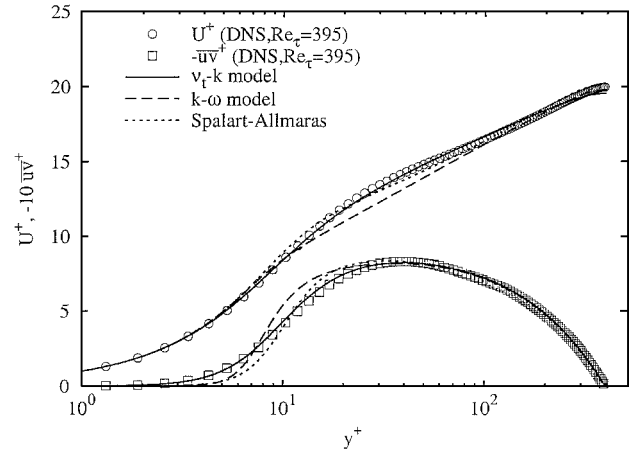

a) Mean velocity and Reynolds stress

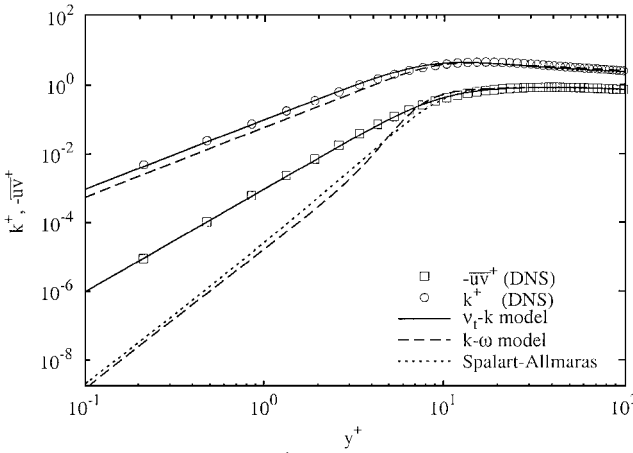

b) Log–log plot of k^+ and $-\overline{uv}^+$

Fig. 1 Fully developed channel flow.

model is applied to analyze the transitional boundary-layer problem, it is impossible to impose the freestream condition that affects the transition significantly. The aim of the present study is to formulate a new ν_t–k model that overcomes these problems of the one-equation model but keeps its advantages.

Model Formulation

When a possibility that there were cross-diffusion terms in k–ε and k–ω equations that are represented by products between gradients of variables k, ε, or ω (Ref. 9) is assumed, a method similar to that used by Menter[8] with an assumption $\sigma_k = \sigma_\varepsilon$ reveals that the most general form of ν_t equation can be written as

$$\frac{\mathrm{D}\nu_t}{\mathrm{D}t} = C_{n1}\frac{\nu_t^2}{k}\left(\frac{\partial U}{\partial y}\right)^2 - C_{n2}k - C_{n3}\left(\frac{\partial \nu_t}{\partial y}\right)^2 + C_{n4}\frac{\nu_t}{k}\frac{\partial k}{\partial y}\frac{\partial \nu_t}{\partial y} + C_{n5}\frac{\nu_t^2}{k^2}\left(\frac{\partial k}{\partial y}\right)^2 + \frac{\partial}{\partial y}\left[\frac{\nu_t}{\sigma_n}\frac{\partial \nu_t}{\partial y}\right] \tag{1}$$

In this equation, the fifth term with $(\partial k/\partial y)^2$ on the right-hand side may be neglected due to its relative smallness in equilibrium and core layers in comparison with other terms. Now, there are five model constants, C_{n1}, C_{n2}, C_{n3}, C_{n4}, and σ_n, to be determined. Because the low-Reynolds-number, turbulent kinetic energy equation in the following form[3] has been widely used and its validity has been well established by a direct numerical simulation (DNS) database, it is adopted in the present study without any modification:

$$\frac{\mathrm{D}k}{\mathrm{D}t} = \nu_t\left(\frac{\partial U}{\partial y}\right)^2 - C_\mu f_\mu \frac{k^2}{\nu_t} + \frac{\partial}{\partial y}\left[\left(\nu + \frac{\nu_t}{\sigma_k}\right)\frac{\partial k}{\partial y}\right] - 2\nu\left(\frac{\partial \sqrt{k}}{\partial y}\right)^2 \tag{2}$$

where $\sigma_k = 1.0$ and $C_\mu = 0.09$. For a high Reynolds number, it is easy to show that the ν_t–k model leads to $k \sim t^{-C_\mu/(C_\mu - C_{n2})}$ for shear-free homogeneous turbulence. Because $k \sim t^{-1.2}$ for high-Reynolds-number turbulence, it is required that $C_{n2} = C_\mu/6$. For high-Reynolds-number homogeneous turbulence with uniform mean shear, the ν_t–k equations yields the following relation:

$$P_k/\varepsilon(1 - C_{n1}) - [1 - (C_{n2}/C_\mu)] = 0 \tag{3}$$

In a summary of 29 experiments on homogeneous uniform shear flow, Tavoularis and Karnik[10] showed that the ratio ε/P_k is nearly constant, and it is independent of the Reynolds number. Taking the mean value of 0.7 for ε/P_k, C_{n1} is determined to be 0.42. Another relation between model constants is obtained from the log layer behavior,[9] which results in

$$C_{n1} - (C_{n2}/C_\mu) + \left(\kappa^2/\sqrt{C_\mu}\right)[(1/\sigma_n) - C_{n3}] = 0 \tag{4}$$

where $\kappa = 0.41$ is the von Kármán constant.

Now, we need two more relations to determine uniquely the model constants, C_{n3}, C_{n4}, and σ_n. These can be found from two arguments: One is the study on the behavior of two-equation models at the edge of a turbulent region by Cazalbou et al.,[11] and the other is the asymptotic form of k in the free boundary edge of a shear-free turbulent mixing layer. With these guides, we obtained that $C_{n3} = 0.95$, $C_{n4} = 1.6$, and $\sigma_n = 2.0$. These constants yield an asymptotic behavior $k \sim y^{-2.78}$ at the edge of a shear-free mixing layer, which is a little steeper than experimental observation.[12] For the near-wall region, because $k \sim y^2$ and $\nu_t \sim y^3$ as $y \to 0$, the molecular diffusion term in Eq. (2) becomes the largest one as $y \to 0$, and it is necessary to make the budget in balance by damping the dissipation term with a damping function f_μ. It is defined that $f_\mu \equiv (\varepsilon - \varepsilon_w)/(C_\mu k^2/\nu_t)$, and $\varepsilon_w = 2\nu(\partial\sqrt{k}/\partial y)^2$. Using DNS data of channel flow at low Reynolds number,[13] f_μ is obtained as

$$f_\mu = 1 - \exp\left[-(R_y/A_1)^3\right] \tag{5}$$

where $R_y = \sqrt{(ky)}/\nu$ and $A_1 = 55$. Next, consider Eq. (1) with a molecular diffusion term for the low-Reynolds-number region. Expand k and ν_t near the wall as

$$k = b_k y^2 + c_k y^3 + \cdots, \qquad \nu_t = c_n y^3 + d_n y^4 + \cdots \tag{6}$$

We find that the molecular diffusion term behaves near the wall as

$$\frac{\partial}{\partial y}\left[\nu\frac{\partial \nu_t}{\partial y}\right] = \nu\left(6c_n y + 12d_n y^2\right) + \cdots \tag{7}$$

which becomes the largest term for $y \to 0$. To counterbalance the budget near the wall, it is necessary to subtract a new term,

$$\frac{8}{3}\nu\left(\frac{\partial \sqrt{\nu_t}}{\partial y}\right)^2 = \nu\left(6c_n y + 10d_n y^2\right) + \cdots \tag{8}$$

This term seems to contribute to the destruction of ν_t by molecular viscosity. When this term is subtracted, the model equations yield too high a level of turbulent kinetic energy in the buffer layer, which is attributed to the next largest two terms that behave as y^2 for $y \to 0$. Damping functions f_{n2} and f_{n4} are, therefore, introduced to these terms to reduce their magnitude near the wall. Numerical optimization is used to find them in the following forms:

$$f_{n2} = 1 - \exp\left[-(R_y/200)^4\right], \qquad f_{n4} = 1 - \exp\left[-(R_y/100)^4\right] \tag{9}$$

Final equations of the proposed ν_t equation is

$$\frac{\mathrm{D}\nu_t}{\mathrm{D}t} = C_{n1}\frac{\nu_t^2}{k}\left(\frac{\partial U}{\partial y}\right)^2 - C_{n2}f_{n2}k - C_{n3}\left(\frac{\partial \nu_t}{\partial y}\right)^2 + C_{n4}f_{n4}\frac{\nu_t}{k}\frac{\partial \nu_t}{\partial y}\frac{\partial k}{\partial y} + \frac{\partial}{\partial y}\left[\left(\nu + \frac{\nu_t}{\sigma_n}\right)\frac{\partial \nu_t}{\partial y}\right] - \frac{8}{3}\nu\left(\frac{\partial \sqrt{\nu_t}}{\partial y}\right)^2 \tag{10}$$

Equations (2) and (10) constitute the new ν_t–k model. These equations with the selected model constants have been used to calculate

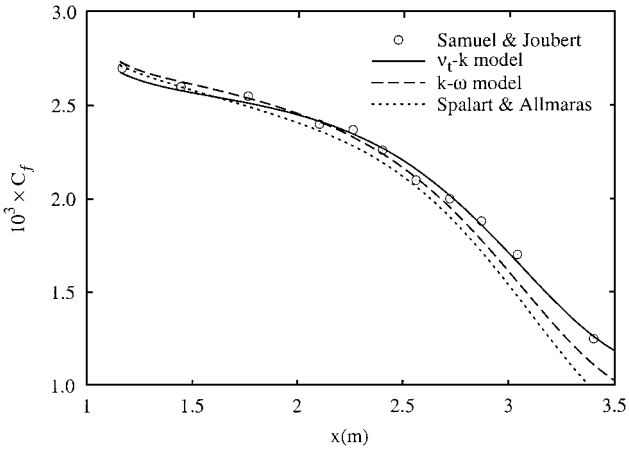

Fig. 2 Friction coefficient in Samuel–Joubert[15] flows.

a fully developed two-dimensional channel flow at $Re_\tau = 395$ (Ref. 13), a flat plate boundary-layer flow,[14] and the boundary-layer flow under adverse pressure gradient.[15]

Applications

Figure 1 shows the comparisons of the predicted U^+, $-\overline{uv}^+$, and k^+ using various models with DNS data. The one-equation model of Spalart and Allmaras[6] and the two-equation model of Wilcox[9] produce slightly larger Reynolds shear stress in the buffer layer, which results in lower velocity profiles in that region. It can be seen that the proposed ν_t–k model yields correct near-wall behavior of the Reynolds shear stress and, thus, the eddy viscosity. Note that other models predict $-\overline{uv}^+ \propto y^4$ as $y \to 0$. The present model is applied to a flat plate boundary layer, which results in good prediction of friction coefficients. A relation, $l = \nu_t/\sqrt{k}$, can infer the turbulence length scale from the ν_t–k model, and it can be seen that the length scale l varies smoothly from zero at the wall to a value in the core region that is similar to that of the conventional algebraic model. For all models considered in this study, the computed skin friction was affected by the location of the first grid point, y_1^+. A comparison of such an influence between k–ε (Ref. 16) and ν_t–k models revealed that a twice larger value of y_1^+ can be used in the ν_t–k model to produce the skin friction within $\pm 1\%$ variation.

Finally, the adverse pressure gradient flow of Samuel and Joubert[15] has been computed. Figure 2 shows that the ν_t–k model best predicts skin-friction coefficients in adverse pressure gradients flows. The predicted velocity and the Reynolds stress profiles, which are not shown here, were also comparable with the experiment.

Conclusions

A new eddy viscosity transport equation is developed to constitute a new ν_t–k model. Natural wall boundary conditions can be used for both ν_t and k equations. Although this model is not free from defects due to the Boussinesq approximation, it yields favorable predictions of a number of standard attached turbulent boundary-layer flows. Further studies are in process to verify the present model for separated flows and compressible flows.

Acknowledgment

This work was supported by a grant from the National Research Laboratory of the Ministry of Science and Technology, Republic of Korea.

References

[1]Baldwin, B. S., and Lomax, H., "Thin-Layer Approximation and Algebraic Model for Separated Turbulent Flows," AIAA Paper 78-257, 1978.

[2]Bradshaw, P., Ferriss, D. H., and Atwell, N. P., "Calculation of Boundary-Layer Development Using the Turbulent Energy Equation," *Journal of Fluid Mechanics*, Vol. 28, 1967, pp. 593–616.

[3]Jones, W. P., and Launder, B. E., "The Prediction of Laminarization with a Two-Equation Model of Turbulence," *International Journal of Heat and Mass Transfer*, Vol. 15, No. 2, 1972, pp. 301–314.

[4]Wilcox, D. C., "Reassessment of the Scale-Determining Equation for Advanced Turbulence Models," *AIAA Journal*, Vol. 26, No. 11, 1988, pp. 1299–1310.

[5]Baldwin, B. S., and Barth, T. J., "A One-Equation Turbulence Transport Model for High Reynolds Number Wall-Bounded Flows," NASA TM-102847, 1990.

[6]Spalart, P. R., and Allmaras, S. R., "A One-Equation Turbulence Model for Aerodynamic Flows," *La Recherche Aérospatiale*, No. 1, 1994, pp. 5–21.

[7]Durbin, P. A., Mansour, N. N., and Yang, Z., "Eddy Viscosity Transport Model for Turbulent Flow," *Physics of Fluids*, Vol. 6, No. 2, 1994, pp. 1007–1015.

[8]Menter, F. R., "Eddy Viscosity Transport Equations and Their Relation to the k–ε Model," *Journal of Fluids Engineering*, Vol. 119, Dec. 1997, pp. 876–884.

[9]Wilcox, D. C., *Turbulence Modeling for CFD*, 2nd ed., DCW Industries, Inc., La Cañada, CA, 1998, pp. 117–149.

[10]Tarvoularis, S., and Karnik, U., "Further Experiments on the Evolution of Turbulent Stresses and Scales in Uniformly Sheared Turbulence," *Journal of Fluid Mechanics*, Vol. 204, 1989, pp. 457–478.

[11]Cazalbou, J. B., Spalart, P. R., and Bradshaw, P., "On the Behavior of Two-Equation Models at the Edge of a Turbulent Region," *Physics of Fluids*, Vol. 6, No. 5, 1994, pp. 1797–1804.

[12]Briggs, D. A., Ferziger, J. H., Koseff, J. R., and Monismith, S. G., "Entrainment in a Shear-Free Turbulent Mixing Layer," *Journal of Fluid Mechanics*, Vol. 310, 1996, pp. 215–241.

[13]Kim, J., Moin, P., and Moser, R., "Turbulence Statistics in Fully Developed Channel Flow at Low Reynolds Number," *Journal of Fluid Mechanics*, Vol. 177, 1987, pp. 133–166.

[14]Kline, S. J., Cantwell, B. J., and Lilley, G. M., *1980-1981 AFOSR-HTTM-Stanford Conference on Complex Turbulent Flows: Comparison of Computation and Experiment*, Stanford Univ., Stanford, CA, 1981, pp. 82–85.

[15]Samuel, A. E., and Joubert, P. N., "A Boundary Layer Developing in an Increasingly Adverse Pressure Gradient," *Journal of Fluid Mechanics*, Vol. 66, 1974, pp. 481–505.

[16]Nagano, Y., and Tagawa, M., "An Improved k–ε Model for Boundary Layer Flows," *Journal of Fluid Engineering*, Vol. 112, 1990, pp. 33–39.

R. M. C. So
Associate Editor

Structural Damage Identification Using Pole/Zero Dynamics in Neural Networks

S. M. Yang* and G. S. Lee†
National Cheng-Kung University, Tainan 701, Taiwan, Republic of China

I. Introduction

EFFECTIVE damage detection and/or identification of structure systems has been the subject of recent studies. The concept is based on that when a structure system undergoes different kinds or degrees of damage, its characteristics will change. A set of structural signatures can then be applied to characterize the damage condition(s). Structural damage identification by artificial neural networks has proven preferable over traditional model-based schemes because of the neural networks, advantages in self-learning, noise insensitivity, fault tolerance, and generalization ability. A feedforward neural network usually has three layers: the input layer, hidden layer, and output layer. From the viewpoint of pattern recognition, a diagnosis network that avoids the complicated algorithms in traditional model-based schemes can construct the mapping of the structural signatures and damage condition. In addition, once an artificial neural network is constructed, it can provide damage identification fast enough for online monitoring.

Received 30 June 1997; revision received 16 April 2001; accepted for publication 26 April 2001.

*Professor, Institute of Aeronautics and Astronautics; smy@mail.iaa.ncku.edu.tw.

†Research Assistant, Institute of Aeronautics and Astronautics.